# Pseudospectral Solutions of One- and Two-Dimensional Inviscid Flows with Shock Waves

Leonidas Sakell*
*Naval Research Laboratory, Washington, D.C.*

**A new approach is presented for the utilization of pseudospectral techniques for the solution of inviscid flows with shock waves using the full Euler equations of motion. Artificial viscosity is applied together with low pass spectral filtering to damp out numerical oscillations that arise ahead of and behind the shock waves. Both second- and fourth-order artificial viscosity schemes are utilized. The fourth-order scheme is shown to be superior. Solutions are presented for the one-dimensional propagating shock wave problem and for two-dimensional supersonic wedge flow. Agreement between the computational results and the analytic solutions is very good.**

## Nomenclature

$A$ = spectral coefficient
$C$ = constant used to evaluate spatial derivative
$c$ = speed of sound
$E$ = axial derivative conservative variables
$e$ = total energy per unit volume
$N$ = total number of collocation points and Chebyshev series terms
$p$ = pressure, nondimensionalized by freestream value
$T$ = Chebyshev polynomial
$t$ = time
$U$ = temporal derivative conservative variables
$u$ = axial velocity, nondimensionalized by freestream sound speed
$x$ = axial direction
$y$ = vertical direction
$\gamma$ = ratio of specific heats
$\eta$ = transformed space vertical coordinate
$\mu$ = artificial viscosity constant
$\xi$ = transformed space axial coordinate
$\rho$ = density, nondimensionalized by freestream value

*Subscripts*

$j$ = collocation point index
$0$ = initial value
$1, 2$ = value at left- and right-hand side computational boundary, respectively

## Introduction

In recent years, spectral and pseudospectral computational techniques have been developed to the point of permitting efficient solution of highly complex incompressible flow problems. These techniques have, for example, been successfully employed to solve for the decay rate of disturbances to the pipe flow of a non-Newtonian fluid, the growth of a turbulent spot in a laminar boundary layer on a flat plate, and a fully developed turbulent channel flow.

In addition, two groups of investigators have recently implemented these techniques to solve the one-dimensional propagating shock wave problem. Taylor et al.[1] and Gottlieb et al.[2] have done so using the time-dependent Euler equations of motion. Each, however, has taken a different approach to control the numerical oscillations which arose. Taylor utilized the flux corrected transport algorithm of Boris and Book.[3] The computations were stable and the shock position was well predicted. However, due to the strength of the smoothing scheme, the shock corners were rounded. Gottlieb et al.[4] developed a filter which was applied directly to the spectral components of the solution. The filter screened out the high-frequency solution components and yielded a stable scheme. The low pass spectral filter did not by itself provide smooth solutions, in that oscillations were still present. To remedy this, a postprocessor Shuman filter was employed. The shock wave location was determined by an examination of the spectral coefficients. Then, the Shuman filter was applied to the flow on either side of the shock front (not across the shock) to yield smooth flow zones together with a sharp shock front.

The present paper describes a third approach to the use of pseudospectral techniques for computing compressible flows with shock waves. Artificial viscosity and a low pass spectral filter are applied throughout the flowfield to control the oscillatory behavior which the solution otherwise has. Solutions for the one-dimensional propagating shock wave and for the two-dimensional wedge flow are presented which agree very well with the analytical solutions of these classical problems. This "hands-off" approach to obtaining sharp shock fronts and correct shock locations appears to be well suited for the solution of more general two- and three-dimensional problems, with multiple discontinuities whose shape and strength are not known a priori.

## Method of Solution

Spectral and pseudospectral methods are expansion function techniques for solving differential equations. They differ in that the Galerkin or the Tau method is employed to relate the expansion function coefficients to the boundary conditions for a spectral method. The pseudospectral approach requires that the differential equation be satisfied only at certain discrete points in the computational domain, called collocation points.

In the present work Chebyshev polynomials are used as the expansion functions. A function $E(x,t)$ is represented as

$$E(x,t)=\sum_{n=0}^{N} A_n(t)T_n(x) \tag{1}$$

That is, the temporal dependence is confined to the expansion function coefficients and the spatial dependence to the expansion functions themselves. The associated collocation points

Received June 21, 1982; revision submitted July 18, 1983. This paper is declared a work of the U.S. Government and therefore is in the public domain.

*Aerospace Engineer, Marine Technology Division, Fluid Dynamics Branch.

are

$$x_j = \cos(\pi j/N), \qquad 0 < j \le N \tag{2}$$

so that

$$E(x_j, t) = \sum_{n=0}^{N} A_n(t)\cos\left(\frac{\pi jn}{N}\right) \tag{3}$$

(As can be seen easily, the collocation points are not evenly spaced but instead are clustered around $x = \pm 1$.) Temporal derivatives may be computed by any one of a number of finite difference algorithms, and in the present work the Adams-Bashforth formulation is used.

The conservation law form of the one-dimensional, unsteady Euler equations is

$$\frac{\partial \boldsymbol{U}}{\partial t} + \frac{\partial \boldsymbol{E}}{\partial x} = 0 \tag{4a}$$

where

$$\boldsymbol{U} = \begin{bmatrix} \rho \\ \rho u \\ e \end{bmatrix}; \qquad \boldsymbol{E} = \begin{bmatrix} \rho u \\ p + \rho u^2 \\ (e+p)u \end{bmatrix} \tag{4b}$$

$$e = \frac{p}{(\gamma - 1)} + \frac{\rho u^2}{2} \tag{4c}$$

$\boldsymbol{E}$ is represented by the series expansion Eq. (3). At any time step $t = t_0$ for which the values of $\boldsymbol{E}(x, t_0)$ are known, the expansion function coefficients $A_n(t_0)$ are obtained by taking the inverse fast Fourier transform (FFT) of Eq. (3). The spatial derivative of $\boldsymbol{E}(x, t_0)$ may be related to the value of the function itself using the well known recursion relationship for Chebyshev polynomials. The result is

$$\frac{\partial \boldsymbol{E}}{\partial x} = \sum_{n=0}^{N} \frac{2}{C_n} \sum_{\substack{p=n+1 \\ p+n=\text{odd}}}^{N} pA_p(t_0) \tag{5}$$

Here $C_n = 2$ for $n = 0$, and $C_n = 1$ otherwise. The summation of Eq. (5) is performed by a direct FFT operation. The temporal derivative of $\boldsymbol{U}(x, t)$ is then obtained for time step $t_0 + \Delta t$ as

$$\boldsymbol{U}^{t_0+\Delta t} = \boldsymbol{U}^{t_0} + \frac{3}{2}\Delta t\left(\frac{\partial \boldsymbol{E}}{\partial x}\right)^{t_0} - \frac{1}{2}\Delta t\left(\frac{\partial \boldsymbol{E}}{\partial x}\right)^{t_0-\Delta t} \tag{6}$$

i.e., the Adams-Bashforth algorithm. Here the superscripts denote the time at which each term was evaluated. (It should be noted that the modified Euler predictor-corrector scheme was also investigated for time differencing. However, it did not yield better results and took more computer time to implement.)

The boundary conditions for the computations are specified as in Refs. 2 and 5. At subsonic inflow boundaries two flow variables are held fixed while the third is calculated from the value of the outgoing characteristic quantity. At subsonic outflow boundaries, one flow variable is specified and the remaining two are determined from the values of the two outgoing characteristic quantities. At supersonic inflow boundaries all flow variables are specified, while at supersonic outflow boundaries nothing is specified.

The integration time step size for pseudospectral calculations has been shown by Gottlieb to satisfy the following condition for numerical stability:

$$\Delta t \le \frac{8.0}{N^2|u + c|_{\max}} \tag{7}$$

We may introduce a Courant number by a simple modification of Eq. (7).

$$\Delta t = \frac{8.0\ \text{CN}}{N^2|u + c|_{\max}} \tag{8}$$

where the Courant number $\text{CN} \le 1$. For all results reported herein, a Courant number of 0.5 was used. No attempt was made to use larger values. The factor $1/N^2$ which appears in Eqs. (7) and (8) represents the minimum point spacing. If the grid interval is changed from $-1 \le x \le +1$ to say $x_1 \le x \le x_2$, then Eq. (8) should be modified to become:

$$\Delta t = \frac{8.0\ \text{CN}\Delta x_{\min}}{|u + c|_{\max}} \tag{9}$$

The second- and fourth-order viscosity formulations employed in the present work were, respectively,

$$D_{n,j} = -\mu\{\boldsymbol{U}_{n,j+1} - 2\boldsymbol{U}_{n,j} + \boldsymbol{U}_{n,j-1}\} \tag{10}$$

$$D_{n,j} = -\mu\{\boldsymbol{U}_{n,j+2} + \boldsymbol{U}_{n,j-2} - 4[\boldsymbol{U}_{n,j+1} + \boldsymbol{U}_{n,j} + \boldsymbol{U}_{n,j-1}] + 6\boldsymbol{U}_{n,j}\} \tag{11}$$

where $D_{n,j}$ is the magnitude of the dissipation term at the $n$th time step and $j$th spatial location. The dissipation constant is given by $\mu$ and $\boldsymbol{U}$ is given by Eq. (4b).

## Computational Results

All calculations were done on the NRL Advanced Scientific Computer utilizing the ASC vector compiler. Run times for the one-dimensional calculations with 128 points were 0.05 s of CPU time per iteration. For the two-dimensional calculations with a $33 \times 33$ grid, run times were 0.023 s of CPU time per iteration.

Results of a one-dimensional propagating shock wave calculation at a single Mach number are first presented to show the relative merit of second- and fourth-order artificial viscosity formulations in pseudospectral calculations. The solutions of additional one-dimensional propagating shock wave and two-dimensional wedge flow calculations, obtained with the superior fourth-order formulation, are then presented.

### Comparison of Second- and Fourth-Order Artificial Viscosities for a One-Dimensional Propagating Shock Wave Calculation

The test problem used to investigate the utility of each scheme for pseudospectral computations was a Mach 1.8 shock wave propagating into a subsonic ($M = 0.5$) freestream. For this case the postshock flow is subsonic and the inflow boundary is subsonic, while the outflow boundary is also subsonic. At the inflow boundary the pressure and velocity were specified and the density computed from the outgoing characteristic quantity. At the outflow boundary, the pressure is specified and the density and velocity are calculated from the incoming characteristic quantities. A total of 128 collocation points (Chebyshev series terms) was used to model the flow. A CN of 0.5, resulting in a time integration step size of $0.99 \times 10^{-4}$, was used.

Results for the density field with second-order smoothing after 5000 time steps are shown in Figs. 1–3. Three different artificial viscosity constants were used, namely: $0.3 \times 10^{-3}$, $0.3 \times 10^{-2}$, $0.3 \times 10^{-1}$. Results at the outflow boundary were well behaved for all viscosity constant values. This was not the case at the inflow boundary. The pressure and velocity were well behaved (they were held fixed) while the density and energy were not. The second-order artificial viscosity scheme provides unacceptable contamination of the solution and should not be used.

The test case was then run using the fourth-order artificial viscosity scheme. Results after 5000 steps are shown in Figs.

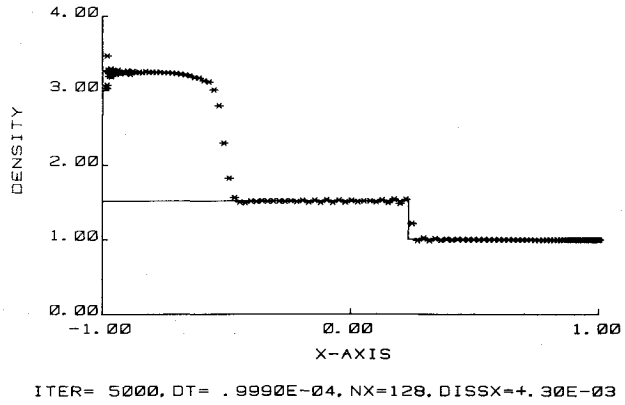


**Fig. 1 Propagating shock wave, second-order smoothing, subsonic inflow and outflow.**

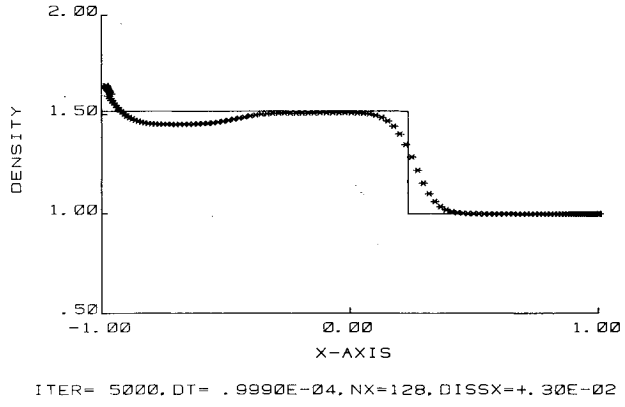


**Fig. 2 Propagating shock wave, second-order smoothing, subsonic inflow and outflow.**

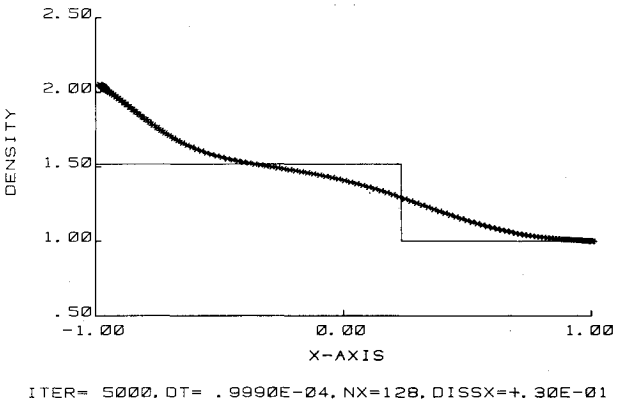


**Fig. 3 Propagating shock wave, second-order smoothing, subsonic inflow and outflow.**

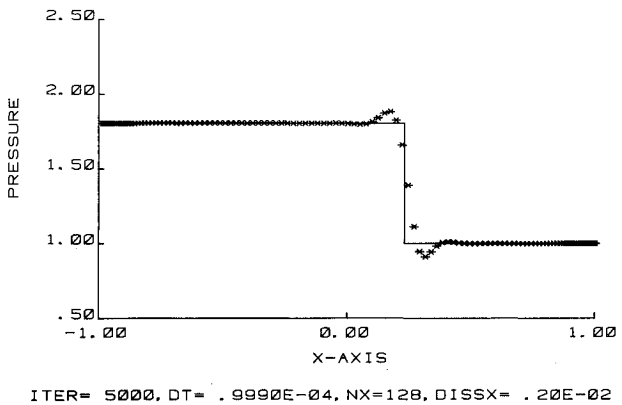


**Fig. 4 Propagating shock wave, fourth-order smoothing, subsonic inflow and outflow.**

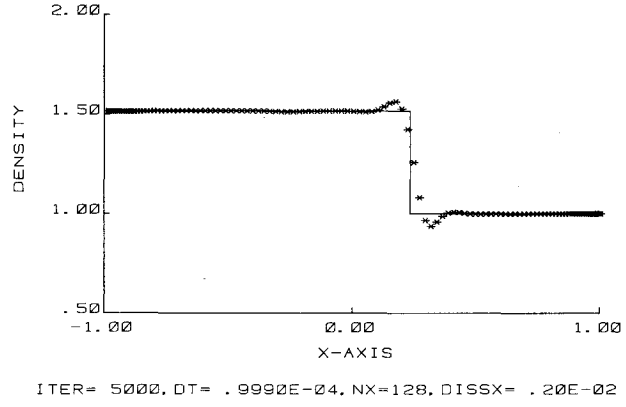


**Fig. 5 Propagating shock wave, fourth-order smoothing, subsonic inflow and outflow.**

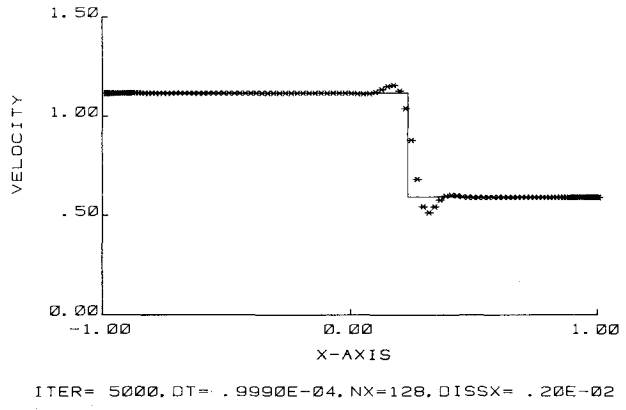


**Fig. 6 Propagating shock wave, fourth-order smoothing, subsonic inflow and outflow.**

4–7. The viscosity constant used was $0.2 \times 10^{-2}$. All flow variables are well behaved at the inflow and outflow boundaries. The fourth-order scheme does not contaminate the solution as does the second-order scheme. Based on these results, the fourth-order scheme was used for all further results reported herein.

### Additional One-Dimensional Propagating Shock Wave Solutions Obtained with the Fourth-Order Artificial Viscosity Formulation

In addition to the test case previously discussed, two additional cases were considered. They were selected so that the Mach numbers at the inflow and outflow boundaries were different from before (subsonic inflow and outflow). In this way, any resolution differences due to the flow at the boundaries could be determined.

Figures 8–11 show results after 4000 time steps for the case of supersonic inflow and subsonic outflow. The freestream Mach number is 0.5, the shock propagation Mach number (with respect to the ground) is 2.949 and 128 points (Chebyshev series terms) were used to resolve the flow. No adverse behavior arises at either boundary. The shock wave is maintained as a discontinuity at the correct location. The comparison between the computed solution (star symbols) and the analytic solution (solid line) is very good. Some minor overshoots and undershoots are present. The rotation of the calculated shock front away from 90 deg is mostly due to the coarse grid spacing which arises in the neighborhood of $x = 0.0$.

Results for the case of supersonic inflow and outflow are shown in Figs. 12–15. The freestream Mach number is 1.5 and the shock propagation Mach number (with respect to ground

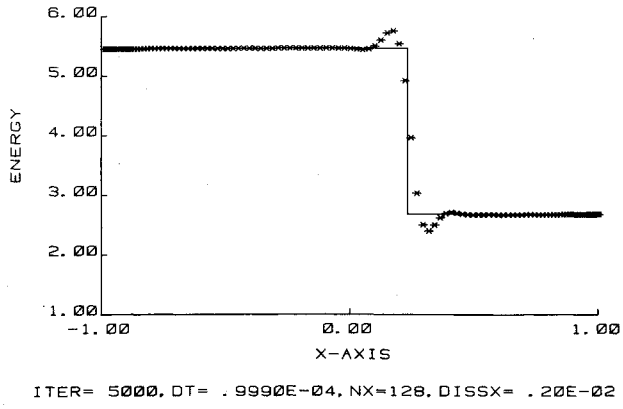


**Fig. 7 Propagating shock wave, fourth-order smoothing, subsonic inflow and outflow.**

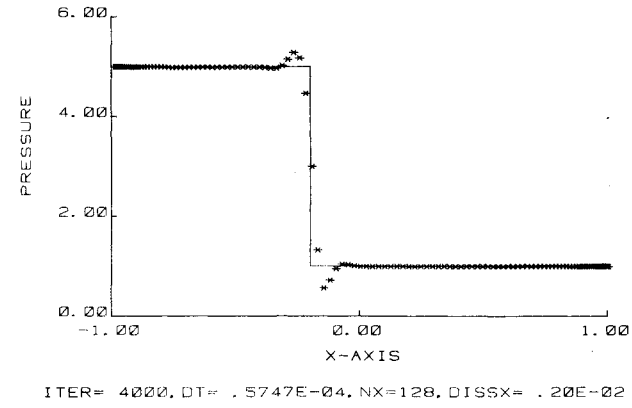


**Fig. 8 Propagating shock wave, fourth-order smoothing, supersonic inflow, and subsonic outflow.**

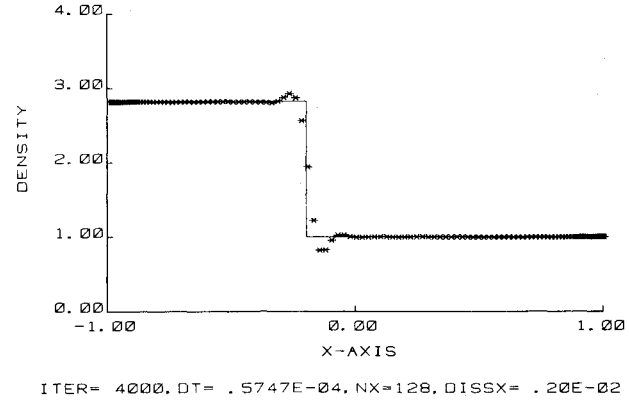


**Fig. 9 Propagating shock wave, fourth-order smoothing, supersonic inflow, and subsonic outflow.**

fixed coordinates) is 3.5. Agreement between the computed solution and the analytic solution is quite good. No adverse affects arise at either boundary.

### Two-Dimensional Wedge Flow Results

To determine the effectiveness of pseudospectral techniques in computing two-dimensional flow, a supersonic wedge flow was considered. The alignment of the computational boundary in physical space is shown in Fig. 16. It is evident that the range in physical coordinates over this boundary is $x_1 \le x \le x_2$ and $0 \le y \le y_{\max}$. Since the collocation points must be bounded by unity in absolute values a coordinate transformation is

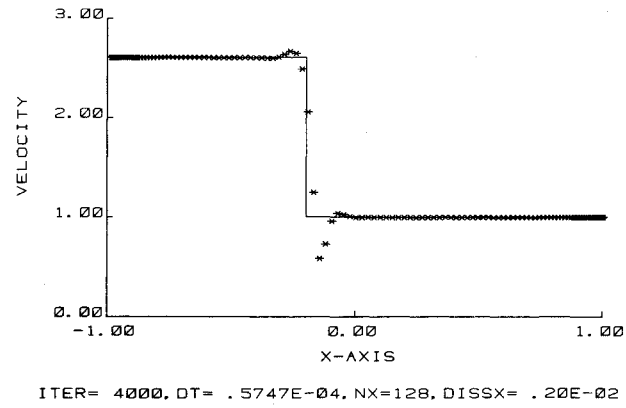


**Fig. 10 Propagating shock wave, fourth-order smoothing, supersonic inflow, and subsonic outflow.**

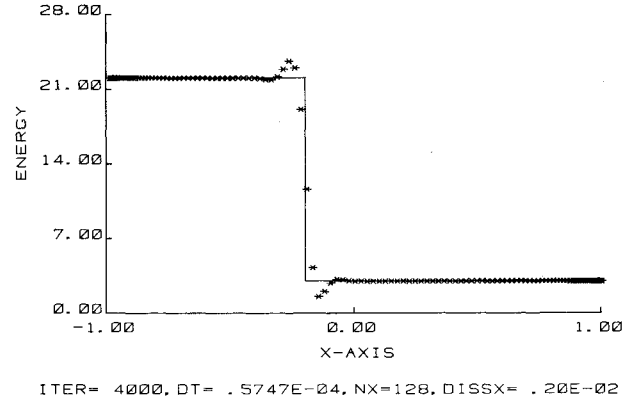


**Fig. 11 Propagating shock wave, fourth-order smoothing, supersonic inflow, and subsonic outflow.**

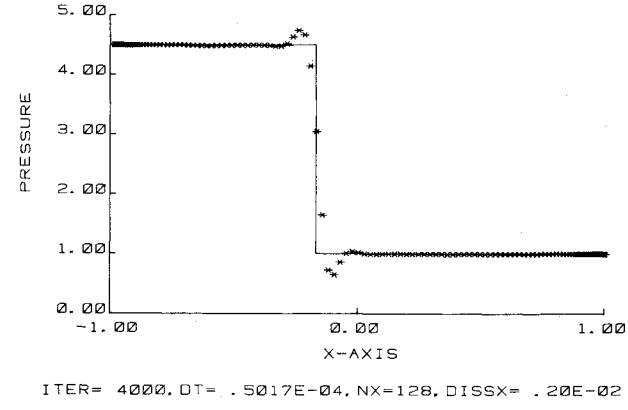


**Fig. 12 Propagating shock wave, fourth-order smoothing, supersonic inflow and outflow.**

introduced:

$$\xi = \frac{2x - (x_1 + x_2)}{(x_2 - x_1)}, \qquad \eta = \frac{2y - y_{\max}}{y_{\max}} \tag{12}$$

where

$$-1 \le \xi \le +1, \qquad -1 \le \eta \le +1$$

as is required. The $\eta$-space transformation above was purposely selected to maintain the wedge shock nonaligned with

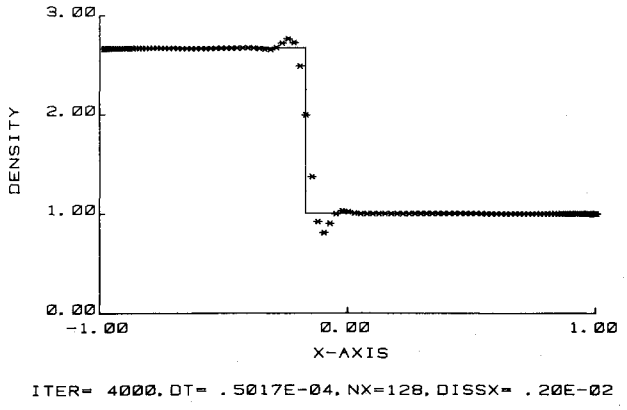


**Fig. 13 Propagating shock wave, fourth-order smoothing, supersonic inflow and outflow.**

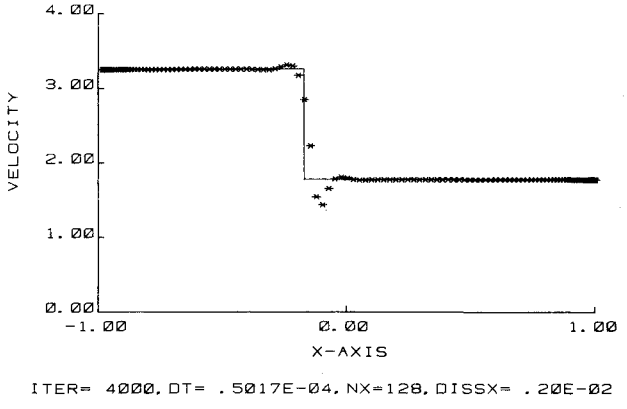


**Fig. 14 Propagating shock wave, fourth-order smoothing, supersonic inflow and outflow.**

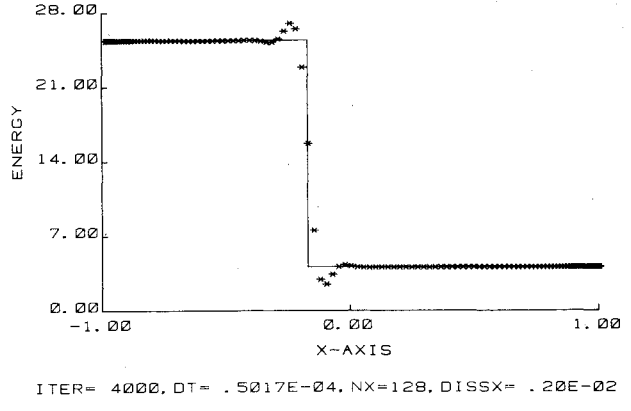


**Fig. 15 Propagating shock wave, fourth-order smoothing, supersonic inflow and outflow.**

respect to a constant $\eta$ line, and thus to maximize the occurrence of pre- and postshock oscillations to allow for a better evaluation of the suitability of the solution technique.

A $33 \times 33$ point grid was used to model the flowfield. The freestream Mach number was 5.0 and the wedge half angle is 10 deg. Supersonic inflow results over the left-hand side and top portion of the computational boundary while supersonic outflow occurs along the right-hand side. As discussed earlier, all flow variables were held fixed at supersonic inflow points and none held fixed at supersonic outflow points. The flow along the computational boundary was initialized to freestream or wedge flow values, and all points interior to the computa-

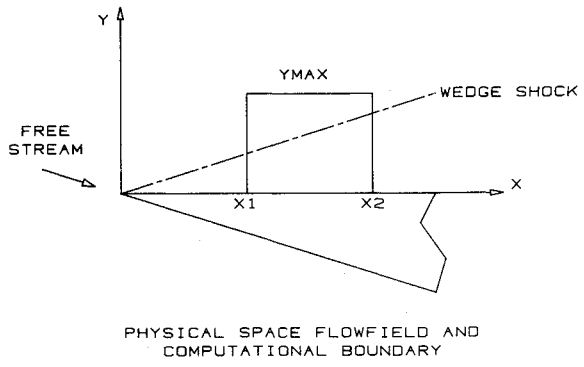


**Fig. 16 Two-dimensional wedge flow.**

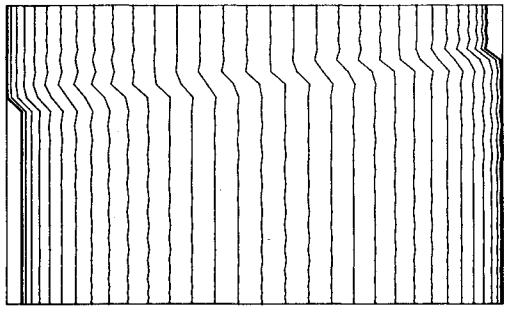


**Fig. 17 Two-dimensional wedge flow pressure field.**

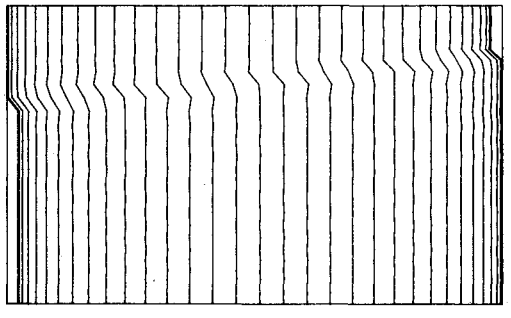


**Fig. 18 Two-dimensional wedge flow density field.**

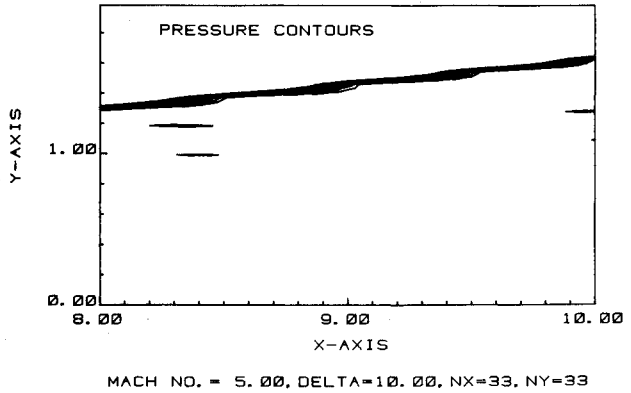


**Fig. 19 Two-dimensional wedge flow pressure contours.**

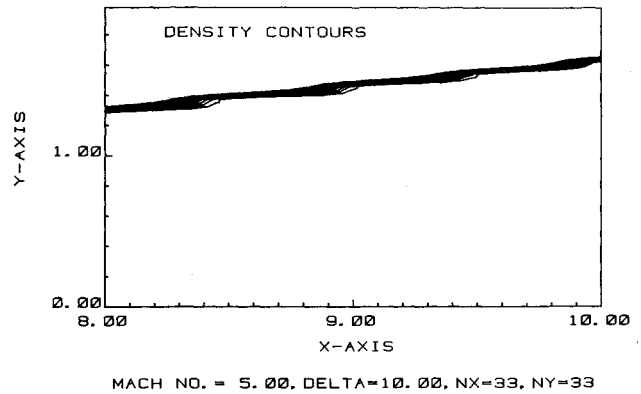


**Fig. 20 Two-dimensional wedge flow density contours.**

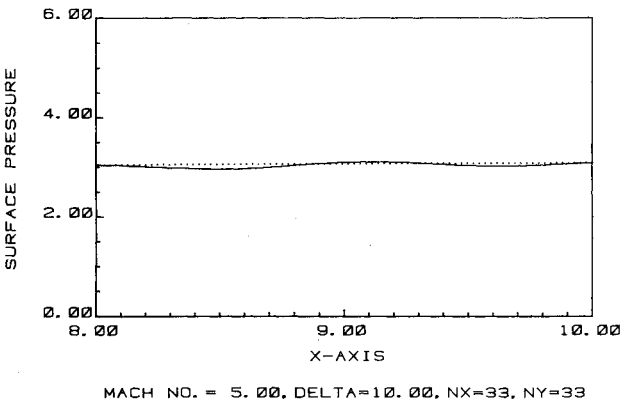


**Fig. 21 Two-dimensional wedge flow surface pressure distribution.**

tional boundary were initialized to freestream values. Along the wedge surface, surface tangency was imposed as a boundary condition.

Results are presented in Figs. 17–22 for the full pressure and density fields, contour plots of pressure and density, and finally the surface pressure and density distributions. One can judge the amount of oscillation that arises in the overall solution from Figs. 17 and 18. Figure 17 shows the pressure raw data and Fig. 18 the density raw data. The amount of oscillation in the overall solution is minimal. It is slightly greater in the pressure field since the pressure is computed from the calculated values of $\rho$, $u$, $v$, and energy $e$. Thus, any oscillations in the calculated flow quantities are magnified in the computation for the pressure. The variation in the sharpness of the jump of flow variables (i.e., different number of points resolving the shock) from line to line is due to the change in shock position within a grid interval which occurs from line to line. (Recall that the shock is not aligned along a constant coordinate direction.)

The resultant shock position and orientation are more readily seen in Figs. 19 and 20. Pressure contours are shown in Fig. 19. There are some minor oscillations, evident by the short contours which appear. The waviness of the main contour arises from the interpolation technique of the contour

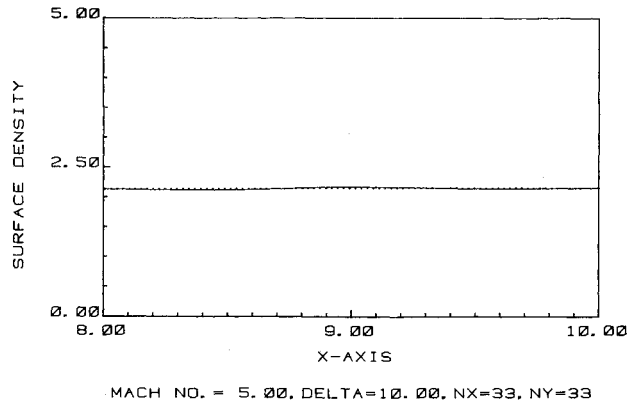


**Fig. 22 Two-dimensional wedge flow surface density distribution.**

plotting program. The wedge shock is correctly positioned and no other discontinuities are present. The same is evident in Fig. 20, where the density field is contoured. There are no contact surfaces or other discontinuities present other than the wedge shock itself. Plots of the surface pressure and density distributions are shown in Figs. 21 and 22. The maximum difference between the computed solution and analytic values is 2.8% in pressure and 1.8% in density. Such resolution is very good for such a coarse ($33 \times 33$) computational grid.

## Conclusions

1) Pseudospectral solution techniques can treat inviscid one- and two-dimensional flows with shock waves quite accurately when a low pass spectral filter is used in conjunction with a fourth-order artificial viscosity scheme (applied to the physical variables). All shocks are maintained as discontinuities with only minor pre- and postcurser oscillations.

2) For one-dimensional propagating shock wave flows, pseudospectral techniques resolve the flow well independently of the Mach number of the flow at the inflow and outflow boundaries.

## Acknowledgment

This work was sponsored by the Office of Naval Research.

## References

[1]Taylor, T., Myers, R., and Albert, J. "Pseudospectral Calculations of Shock Waves. Rarefaction Waves and Contact Surfaces," *Computers and Fluids*, Vol. 9, No. 4, 1981.

[2]Gottlieb, D., Lustman, L., and Orszag, S., "Spectral Calculations of One-Dimensional Inviscid Compressible Flows," *SIAM Journal*, Vol. 2, No. 3, Sept. 1981.

[3]Boris, J. and Book, D., "Solution of Continuity Equations by the Method of Flux-Corrected Transport," *Methods in Computational Physics*, Vol. 16, Academic Press, New York, 1976.

[4]Gottlieb, D. and Orszag, S., *Numerical Analysis of Spectral Methods: Theory and Applications*, CBMS-NSF Regional Conference Series in Applied Mathematics, Monograph 26, 1977.

[5]Gottlieb, D., Gunzburger, M., and Turkel, E., "On Numerical Boundary Treatment of Hyperbolic Systems for Finite Difference and Finite Element Methods," *SIAM Journal*, Vol. 19, Aug. 1982, pp. 671-682.